

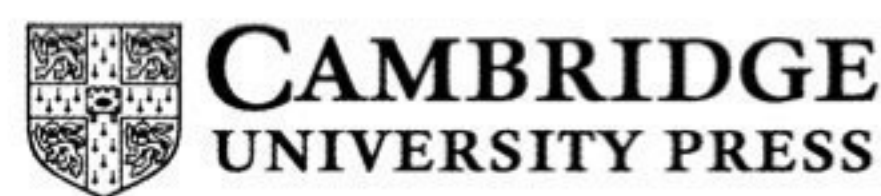
# SOLAR SYSTEM DYNAMICS

CARL D. MURRAY

Queen Mary and Westfield College,  
University of London

STANLEY F. DERMOTT

University of Florida, Gainesville



CAMBRIDGE UNIVERSITY PRESS  
Cambridge, New York, Melbourne, Madrid, Cape Town, Singapore,  
São Paulo, Delhi, Dubai, Tokyo

Cambridge University Press  
32 Avenue of the Americas, New York, NY 10013-2473, USA

[www.cambridge.org](http://www.cambridge.org)  
Information on this title: [www.cambridge.org/9780521575973](http://www.cambridge.org/9780521575973)

© Carl D. Murray and Stanley F. Dermott 1999

This publication is in copyright. Subject to statutory exception  
and to the provisions of relevant collective licensing agreements,  
no reproduction of any part may take place without the written  
permission of Cambridge University Press.

First published 1999  
Reprinted 2001, 2004, 2005, 2006, 2008

*A catalog record for this publication is available from the British Library*

*Library of Congress Cataloging in Publication data*

Murray, Carl D.  
Solar system dynamics / Carl D. Murray, Stanley F. Dermott.  
p. cm.  
ISBN 0-521-57295-9 (hc.). – ISBN 0-521-57597-4 (pbk.)  
1. Solar system. 2. Celestial mechanics. I. Dermot, S. F.  
II. Title.  
QB500.5.M87 1999  
523.2 – dc21 99-19679  
CIP

ISBN 978-0-521-57295-8 Hardback  
ISBN 978-0-521-57597-3 Paperback

Transferred to digital printing 2009

Cambridge University Press has no responsibility for the persistence or  
accuracy of URLs for external or third-party Internet websites referred to in  
this publication, and does not guarantee that any content on such websites is,  
or will remain, accurate or appropriate. Information regarding prices, travel  
timetables and other factual information given in this work are correct at  
the time of first printing but Cambridge University Press does not guarantee  
the accuracy of such information thereafter.

Acht chena is álaind cech nderg,  
is gel cach núá,  
is caín cech ard, is serb cech gnáth.  
Caíd cech n-écmais, is faill cech n-aichnid  
co festar cech n-éolas.

All that is red is beautiful,  
and all that is new is bright,  
all that is high is lovely, all that is familiar is bitter.  
The unknown is honoured, the known is neglected,  
until all knowledge is known.

Anonymous, Irish, ninth century, *The Sick-Bed of Cú Chulainn*

**In Memory of**

**Frank Murray**

He was a man, take him for all in all,  
I shall not look upon his like again.

William Shakespeare, *Hamlet, I, ii*

and

**Geraldine Murphy**

At the end we preferred to travel all night,  
Sleeping in snatches  
With the voices singing in our ears, saying  
That this was all folly.

T. S. Eliot, *Journey of the Magi*

# Contents

<i>Preface</i>	xiii
<b>1 Structure of the Solar System</b>	<b>1</b>
1.1 Introduction	1
1.2 The Belief in Number	2
1.3 Kepler's Laws of Planetary Motion	3
1.4 Newton's Universal Law of Gravitation	4
1.5 The Titius–Bode “Law”	5
1.6 Resonance in the Solar System	9
1.7 The Preference for Commensurability	15
1.8 Recent Developments	17
Exercise Questions	19
<b>2 The Two-Body Problem</b>	<b>22</b>
2.1 Introduction	22
2.2 Equations of Motion	23
2.3 Orbital Position and Velocity	25
2.4 The Mean and Eccentric Anomalies	32
2.5 Elliptic Expansions	37
2.6 The Guiding Centre Approximation	42
2.7 Barycentric Orbits	45
2.8 The Orbit in Space	48
2.9 Perturbed Orbits	54
2.10 Hamiltonian Formulation	57
Exercise Questions	60
<b>3 The Restricted Three-Body Problem</b>	<b>63</b>
3.1 Introduction	63
3.2 Equations of Motion	64
3.3 The Jacobi Integral	68

3.4	The Tisserand Relation	71
3.5	Lagrangian Equilibrium Points	74
3.6	Location of Equilibrium Points	77
3.7	Stability of Equilibrium Points	83
3.8	Motion near $L_4$ and $L_5$	95
3.9	Tadpole and Horseshoe Orbits	97
3.10	Orbits and Zero-Velocity Curves	102
3.11	Trojan Asteroids and Satellites	107
3.12	Janus and Epimetheus	110
3.13	Hill's Equations	115
3.14	The Effects of Drag	121
	Exercise Questions	128
<b>4</b>	<b>Tides, Rotation, and Shape</b>	<b>130</b>
4.1	Introduction	130
4.2	The Tidal Bulge	131
4.3	Potential Theory	136
4.4	Tidal Deformation	140
4.5	Rotational Deformation	149
4.6	The Darwin–Radau Relation	153
4.7	Shapes and Internal Structures of Satellites	155
4.8	The Roche Zone	158
4.9	Tidal Torques	160
4.10	Satellite Tides	166
4.11	Tidal Heating of Io	174
4.12	Tides on Titan	175
4.13	Tidal Evolution	178
4.14	The Double Synchronous State	183
	Exercise Questions	186
<b>5</b>	<b>Spin–Orbit Coupling</b>	<b>189</b>
5.1	Introduction	189
5.2	Tidal Despinning	189
5.3	The Permanent Quadrupole Moment	194
5.4	Spin–Orbit Resonance	200
5.5	Capture into Resonance	210
5.6	Forced Librations	215
5.7	Surface of Section	217
	Exercise Questions	222
<b>6</b>	<b>The Disturbing Function</b>	<b>225</b>
6.1	Introduction	225
6.2	The Disturbing Function	226
6.3	Expansion Using Legendre Polynomials	228

6.4	Literal Expansion in Orbital Elements	233
6.5	Literal Expansion to Second Order	238
6.6	Terms Associated with a Specific Argument	246
6.7	Use of the Disturbing Function	248
6.8	Lagrange's Planetary Equations	251
6.9	Classification of Arguments in the Disturbing Function	253
6.10	Sample Calculations of the Averaged Disturbing Function	261
6.11	The Effect of Planetary Oblateness	264
	Exercise Questions	270
<b>7</b>	<b>Secular Perturbations</b>	<b>274</b>
7.1	Introduction	274
7.2	Secular Perturbations for Two Planets	274
7.3	Jupiter and Saturn	279
7.4	Free and Forced Elements	283
7.5	Jupiter, Saturn, and a Test Particle	289
7.6	Gauss's Averaging Method	293
7.7	Generalised Secular Perturbations	299
7.8	Secular Theory for the Solar System	302
7.9	Generalised Free and Forced Elements	307
7.10	Hirayama Families and the <i>IRAS</i> Dust Bands	309
7.11	Secular Resonance	314
7.12	Higher Order Secular Theory	317
	Exercise Questions	318
<b>8</b>	<b>Resonant Perturbations</b>	<b>321</b>
8.1	Introduction	321
8.2	The Geometry of Resonance	321
8.3	The Physics of Resonance	326
8.4	Variation of Orbital Elements	328
8.5	Resonance in the Circular Restricted Three-Body Problem	332
8.6	The Pendulum Model	334
8.7	Libration Width	337
8.8	The Hamiltonian Approach	341
8.9	The 2:1 Resonance	364
8.10	The 3:1 and 7:4 Resonances	371
8.11	Additional Resonances and Resonance Splitting	373
8.12	Resonant Encounters	375
8.13	The Dynamics of Capture and Evolution in Resonance	385
8.14	Two-Body Resonances in the Solar System	387
8.15	Resonant Encounters in Satellite Systems	390
8.16	Three-body Resonance	394
8.17	The Laplace Resonance	396

8.18	Secular and Resonant Motion	399
8.19	LONGSTOP Uranus	402
8.20	Pulsar Planets	405
	Exercise Questions	406
<b>9</b>	<b>Chaos and Long-Term Evolution</b>	<b>409</b>
9.1	Introduction	409
9.2	Sensitive Dependence on Initial Conditions	410
9.3	Regular and Chaotic Orbits	413
9.4	Chaos in the Circular Restricted Problem	421
9.5	Algebraic Mappings	428
9.6	Separatrices and Resonance Overlap	448
9.7	The Rotation of Hyperion	452
9.8	The Kirkwood Gaps	456
9.9	The Neptune-Pluto System	466
9.10	The Stability of the Solar System	469
	Exercise Questions	471
<b>10</b>	<b>Planetary Rings</b>	<b>474</b>
10.1	Introduction	474
10.2	Planetary Ring Systems	475
10.3	Resonances in Rings	481
10.4	Density Waves and Bending Waves	492
10.5	Narrow Rings and Sharp Edges	495
10.6	The Encke Gap and Pan	512
10.7	The F Ring of Saturn	515
10.8	The Adams Ring of Neptune	518
10.9	The Evolution of Rings	520
10.10	The Earth's Dust Ring	522
	Exercise Questions	524
	<b>Appendix A: Solar System Data</b>	<b>526</b>
A.1	Introduction	526
A.2	Astronomical Constants	526
A.3	Julian Date	527
A.4	Orbital Elements of the Planets and Their Variation	529
A.5	Planets, Satellites, and Rings	530
A.6	Asteroids, Centaurs, Trans-Neptunian Objects, and Comets	535
	<b>Appendix B: Expansion of the Disturbing Function</b>	<b>539</b>
	<i>References</i>	557
	<i>Index</i>	577

# 9

## Chaos and Long-Term Evolution

Take but degree away, untune that string,  
And hark what discord follows. Each thing meets  
In mere oppugnancy.

William Shakespeare, *Troilus and Cressida*, I, iii

### 9.1 Introduction

In this book we have derived a number of equations of motion to study the rotational and orbital motion of solar system objects. These equations have described either conservative systems, such as the two- and three-body problems, or dissipative systems, such as the equations governing tidal evolution or the dynamical effects of drag forces. However, all have a common characteristic: They describe systems that are *deterministic*. This means that the current state of the system allows us to calculate its past and future state providing we know all the forces that are acting on it. In the case of the two-body problem we were able to solve the equations of motion and calculate the behaviour of the system at all past and future times. A complete analytical solution was not possible in the case of the three-body problem and we had to rely on numerical solutions if we wanted to follow the orbital evolution of a test particle. However, there was an implicit assumption that, given the initial state of the system, we should be able to calculate its future state by obtaining solutions of the equations of motion. Unfortunately this assumption is not valid for some of the systems we have investigated and this is because of the phenomenon called *chaos*.

In Chapter 7 we saw how the simple assumptions of secular perturbation theory allowed us to derive an analytical solution to the problem of the mutual interaction of  $N$  masses. Although we gained no information about the positions of bodies on their orbits we could at least calculate the other orbital elements at any time, past or present, from knowledge of the current values. The solution of the secular problem by Laplace allowed him to make assertions about the

long-term stability of the solar system. Laplace himself believed in a deterministic universe where once the laws of nature had been discovered, it would only be a matter of knowing all the initial conditions and solving the appropriate equations; then everything about the system would be known. We now know that this view is false.

In the late nineteenth century Henri Poincaré, now acknowledged as the founder of the science of nonlinear dynamics, began a study of the mathematics of the three-body problem. This seminal work, eventually published in his *Les Méthodes Nouvelles de la Mécanique Céleste*, (Poincaré 1892, 1893, 1899), hinted at the complicated nature of the motion that can arise in solutions to the problem. Poincaré had realized that some starting conditions can give rise to unusual trajectories and laid a solid mathematical foundation for the study of chaos.

The major drawback to numerical studies in Poincaré's time was the lack of an efficient means of obtaining solutions to the equations of motion. The advent of digital computers with ever-increasing performances has added an experimental approach to the whole study of nonlinear dynamics in general, and solar system dynamics in particular. Combined with new observations and advances in theory, this means that we can now recognize the important role that chaos has played in determining the dynamical structure and evolution of the solar system.

There is still no universally accepted definition of chaos, even though it can be detected in a variety of dynamical systems. However, for our purposes we can make use of the following definition: An object in the solar system can be said to exhibit chaotic motion if its final dynamical state is sensitively dependent on its initial state. Given that the measure of any physical quantity has a built-in error, the lack of precision in starting conditions is transformed into an uncertainty in final conditions. In this chapter we examine the nature and consequences of chaotic phenomena in the context of long-term dynamical evolution. The article by Murray (1998) provides a summary of the major results in this field.

## 9.2 Sensitive Dependence on Initial Conditions

Consider the motion of a test particle in the vicinity of a planet orbiting the Sun. If the planet is in a circular orbit then this is an example of the circular restricted three-body problem. In the planar case the components of the particle's osculating position and velocity vectors at any time define four quantities,  $x$ ,  $y$ ,  $\dot{x}$ , and  $\dot{y}$ , which give the particle a unique "position" in a four-dimensional space referred to as *phase space*. As the particle evolves it follows a trajectory in phase space as well as the usual *configuration space* consisting of its motion in the  $x$ - $y$  plane. If the particle experiences only the gravitational field of the Sun then its motion would be entirely predictable. However, the perturbations from the planet cause certain regions of the phase space to become chaotic; the

orbital evolution of test particles placed in such regions will take place in an unpredictable fashion.

Figure 9.1 illustrates this phenomenon for two nearby starting conditions for the orbit of a test particle perturbed by Jupiter in the planar, circular restricted problem. Both orbits take the test particle close to Jupiter and yet a difference of only  $0.3^\circ$  in initial longitude is sufficient to produce a dramatically different outcome. This is an example of what is called the *butterfly effect*. This was first mentioned in the context of chaotic weather systems, whereby it was suggested that under suitable conditions the flapping of a butterfly's wings in one part of the world could ultimately lead to a hurricane elsewhere in the world. In the context of solar system dynamics the test particle can be thought of as a spacecraft receiving a gravity assist from a Jupiter flyby. In such examples of chaos a small change in starting values changes the geometry of the encounter and hence the size of the direct perturbation received from the planet.

Comets and asteroids with sufficiently large eccentricities can intersect planetary orbits. With a semi-major axis  $a = 13.75$  AU and an eccentricity  $e = 0.385$ , asteroid (2060) Chiron (see entry in Table A.17) has a perihelion distance inside the orbit of Saturn and an aphelion distance close to the orbit of Uranus. Using the best available orbital elements Oikawa & Everhart (1979) carried out several numerical integrations of Chiron's orbit, all based on starting conditions close to the accepted values. These showed that Chiron will undergo several close approaches to planets. Based on the fact that different starting conditions showed different outcomes, a characteristic of chaotic motion, Oikawa & Everhart were only able to take a probabilistic approach to determining the ultimate fate of

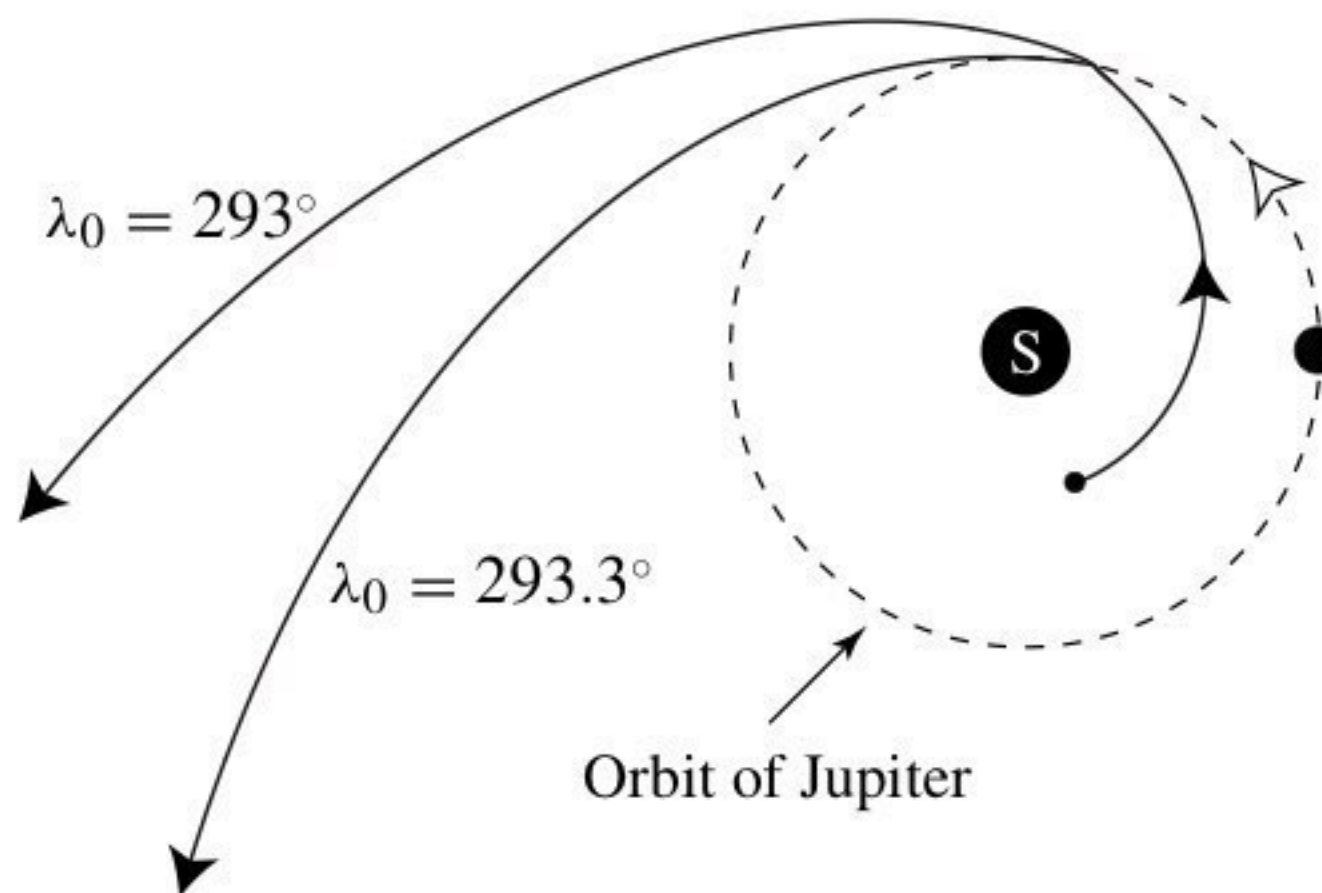


Fig. 9.1. The trajectories of two test particles started with the same semi-major axis ( $a_0 = 0.8$ ), eccentricity ( $e_0 = 0.4$ ), and longitude of pericentre ( $\varpi = 295^\circ$ ) but with slightly different initial mean longitudes ( $\lambda_0 = 293^\circ$  and  $\lambda_0 = 293.3^\circ$ ). Jupiter's orbit is denoted by a dashed circle and it has zero initial longitude. The numerical integration lasted one Jupiter period.

Chiron. They estimated a 1 in 8 chance that Saturn will place Chiron on to a hyperbolic orbit that ejects it from the solar system. The more likely outcome (a 7 in 8 chance) is that the close approaches to Saturn will cause Chiron's orbit to evolve towards the inner solar system where it would come under gravitational perturbations from Jupiter. The classification of Chiron as an asteroid is now debatable with the discovery of large, nonperiodic changes in its brightness (Tholen et al. 1988) and a coma (Meech & Belton 1989). Chiron is now classified as a *Centaur*, one of a number of giant, planet-crossing, cometlike objects that may represent Edgeworth–Kuiper belt objects on their way to becoming short-period comets (see, for example, Luu 1994).

Another example of the butterfly effect in the context of solar system dynamics is the orbital history of Comet Shoemaker-Levy 9. Numerical integrations of the comet's orbit show that prior to its impact with Jupiter in July 1994, it was disrupted by a close approach to Jupiter in 1992. Work by Chodas & Yeomans (1996) suggests that the comet was originally captured into orbit around Jupiter in  $1929 \pm 9$  y. Prior to capture its orbit was probably similar to that of many of the Jupiter family of comets, with a low-eccentricity orbit that was likely to have been interior to Jupiter's orbit. Further information about the history of the comet is impossible, because (i) the orbit is chaotic and (ii) there will be no new astrometric data to enable an improved initial orbit to be determined.

However, chaos can be more subtle. Figure 9.2 shows the results of two numerical integrations of the equations of motion in the circular restricted three-body problem. In this case the orbital evolution is almost exactly the same for approximately 150 Jupiter periods, after which they gradually differ. There is no obvious reason for the drift (for example, there are no close approaches to Jupiter during the integration period) but the behaviour is again characteristic of chaotic motion with the orbits showing a sensitive dependence on initial conditions.

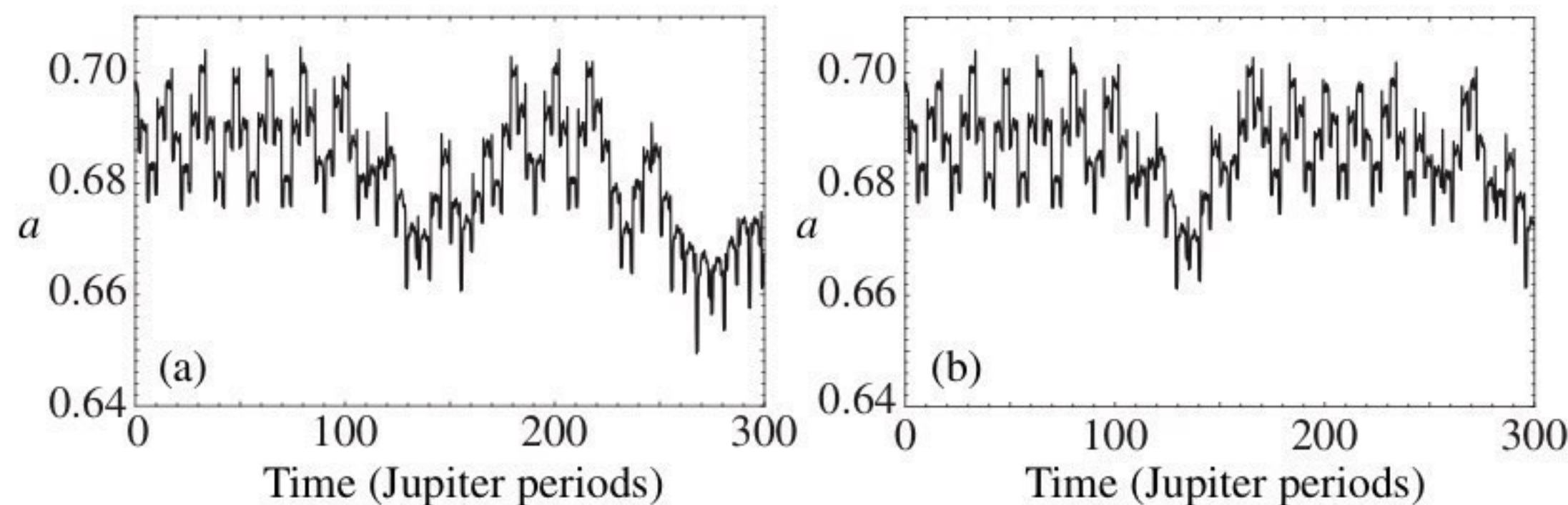


Fig. 9.2. The variation in semi-major axis of two test particles perturbed by Jupiter ( $\mu_2 = 0.001$ ) in the planar, circular restricted problem. The particles were started with the same semi-major axis ( $a_0 = 0.6984$ ), eccentricity ( $e_0 = 0.1967$ ), and longitude of pericentre ( $\varpi = 0^\circ$ ) but with slightly different initial mean longitudes ((a)  $\lambda_0 = 0^\circ$  and (b)  $\lambda_0 = 10^{-6}^\circ$ ). Jupiter was started with zero initial longitude.

The type of chaotic behaviour contrasts with the more dramatic example shown above (see Fig. 9.1) and yet both are valid illustrations of chaos in the circular restricted problem.

### 9.3 Regular and Chaotic Orbits

We have already seen that the two-body problem is integrable (see Chapter 2) whereas the three-body problem is not (see Chapter 3). In fact there are chaotic solutions to the restricted three-body problem for certain starting conditions but we have deliberately avoided discussing them up to this point. We shall carry out a more thorough examination of chaos in the context of the circular, restricted problem in Sect. 9.4. Before proceeding with these and other examples of chaotic motion in the solar system, we demonstrate the differences between regular (i.e., nonchaotic) motion and chaotic motion, showing the characteristics of each and how some of the properties of chaotic orbits can be quantified.

#### 9.3.1 The Poincaré Surface of Section

We met the concept of a surface of section in Sect. 5.4 when we discussed spin-orbit resonance. In that case we were representing the solution of a second-order, nonlinear differential equation for the time variation of  $\theta$ , the orientation angle of a nonspherical satellite. In Fig. 5.17b and 5.18b we plotted points denoting the values of  $\dot{\theta}/n$  and  $\theta$  at every pericentre passage, where  $n$  was the mean motion of the satellite.

In the case of the planar, circular, restricted three-body problem the situation is more complicated. The equations of motion given in Eqs. (3.16) and (3.17) consist of two, simultaneous, nonlinear, second-order differential equations. The equations are repeated here for convenience:

$$\ddot{x} - 2n\dot{y} - n^2x = -\mu_1 \frac{x + \mu_2}{r_1^3} + \mu_2 \frac{x - \mu_1}{r_2^3}, \quad (9.1)$$

$$\ddot{y} + 2n\dot{x} - n^2y = -\left(\frac{\mu_1}{r_1^3} + \frac{\mu_2}{r_2^3}\right)y, \quad (9.2)$$

where  $\mu_1 = m_1/(m_1 + m_2)$ ,  $\mu_2 = m_2/(m_1 + m_2)$ , and

$$r_1^2 = (x + \mu_2)^2 + y^2, \quad (9.3)$$

$$r_2^2 = (x - \mu_1)^2 + y^2, \quad (9.4)$$

where  $r_1$  and  $r_2$  are the distances of the test particle from the masses  $m_1$  and  $m_2$  respectively.

The solution consists of sets of values of  $x$ ,  $y$ ,  $\dot{x}$ , and  $\dot{y}$  at a sequence of times, where these quantities denote the components of the position and velocity vectors in the rotating reference frame. Recall that apart from special starting conditions the restricted problem is nonintegrable and we have to resort to numerical solutions of the equations of motion.

We showed in Chapter 3 that there exists a constant of the motion, the Jacobi constant, defined by

$$C_J = n^2 \left( x^2 + y^2 \right) + 2 \left( \frac{\mu_1}{r_1} + \frac{\mu_2}{r_2} \right) - \dot{x}^2 - \dot{y}^2. \quad (9.5)$$

We have already discussed how the values of  $x$ ,  $y$ ,  $\dot{x}$ , and  $\dot{y}$  at any given time correspond to a single point in a four-dimensional phase space. Because of the existence of the Jacobi constant in the circular restricted problem the path of the particle in phase space is confined to a surface (see Fig. 9.3a). Therefore, for a given, fixed value of the Jacobi constant we only require three out of the four quantities to define the osculating orbit at that time uniquely. This is because the other quantity can be determined, at least up to a sign change, by the equation defining the Jacobi constant. For example, if we take  $x$ ,  $y$ , and  $\dot{x}$  as our three quantities, the other one,  $\dot{y}$ , is determined by Eq. (9.5) (see Fig. 9.3b), provided we have noted the value of the Jacobi constant at time  $t = 0$ . If we now define a plane, say  $y = 0$ , in the resulting three-dimensional space, the values of  $x$  and  $\dot{x}$  can be plotted every time the particle has  $y = 0$  (see Fig. 9.3c). The ambiguity in the sign of  $\dot{y}$  is removed by considering only those crossings with a fixed sign of  $\dot{y}$ . This is the method of the *Poincaré surface of section* or the *Poincaré map* and this is the technique we have used to illustrate the regular and chaotic regions in the circular restricted problem. The section is obtained by fixing a plane in the phase space and plotting the points when the trajectory intersects this plane in a particular direction. Note that as a result we do not plot the points at equal time intervals; we only plot a point when an intersection takes place.

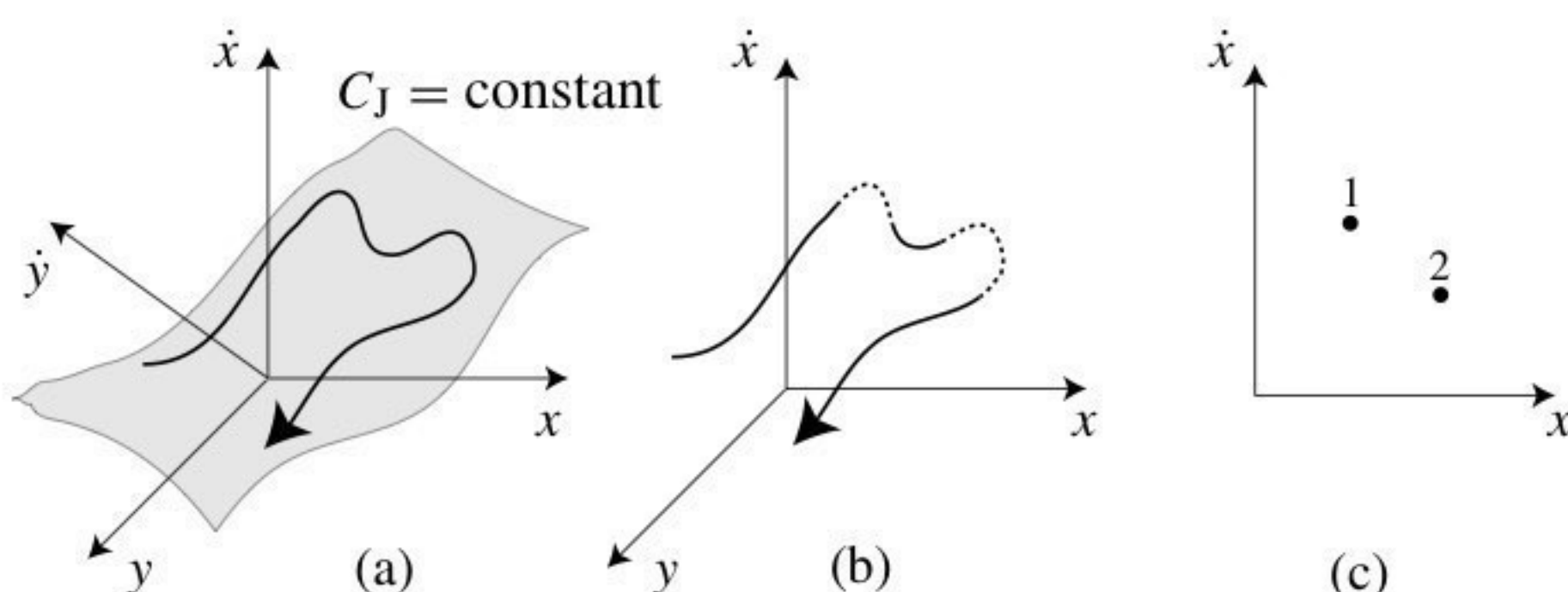


Fig. 9.3. The production of a Poincaré surface of section. (a) The position and velocity of the particle define a point in a four-dimensional phase space at any particular time. The existence of the Jacobi constant means that the test particle's path is moving on a particular surface in this space. (b) We can consider just the  $x$ ,  $y$ , and  $\dot{x}$  values, since the value of  $\dot{y}$  is always determined up to an arbitrary sign change by Eq. (9.5). The dashed line denotes the part of the trajectory where  $y < 0$ . (c) A point is plotted every time  $y = 0$  with  $\dot{y} > 0$ , resulting in a sequence of points in a two-dimensional space.

At first glance we seem to have removed, or at least hidden, a lot of information about the orbit. However, the main advantage of the surface of section method is this very sparseness. Instead of plotting the trajectory in  $x$ - $y$  space and following the test particle around numerous orbits, which may only change slightly, with the surface of section method we get an overview of changes in the orbit. All the information is still contained within those points, even though some effort may be required to extract it. There are other advantages to the method.

We are able to use this technique because we are considering the circular, planar, restricted problem. If we now assume that the eccentricity of the secondary mass is nonzero then we can no longer make use of a Poincaré surface of section for the problem. However, we can make use of the averaging principle and isolate only those terms in an expansion of the disturbing function that are likely to dominate. In some circumstances it is possible to obtain analytical solutions of the averaged system and this was one of the techniques employed in our study of resonant perturbations in the previous chapter.

Now we consider numerical solutions to our system of equations using  $\mu_2 = 10^{-3}$ , a value comparable to the Jupiter/Sun mass ratio.

### 9.3.2 Regular Orbits

Consider the trajectory of a test particle with starting values  $x_0 = 0.55$ ,  $y_0 = 0$ , and  $\dot{x}_0 = 0$ , with  $\dot{y} > 0$  determined from the solution of Eq. (9.5) with  $C_J = 3.07$ . We can convert these values to their equivalent semi-major axis  $a$  and eccentricity  $e$  using the formulae given in Chapter 2. This gives  $a_0 = 0.6944$  and  $e_0 = 0.2065$  for the initial values. In the Sun–Jupiter system this value of  $a_0$  would correspond to a test particle at 3.612 AU, well beyond the main belt of asteroids.

In Fig. 9.4a we show the evolution of  $e$  as a function of time. Although there are obvious variations, the plot shows a regular variation in the eccentricity in the

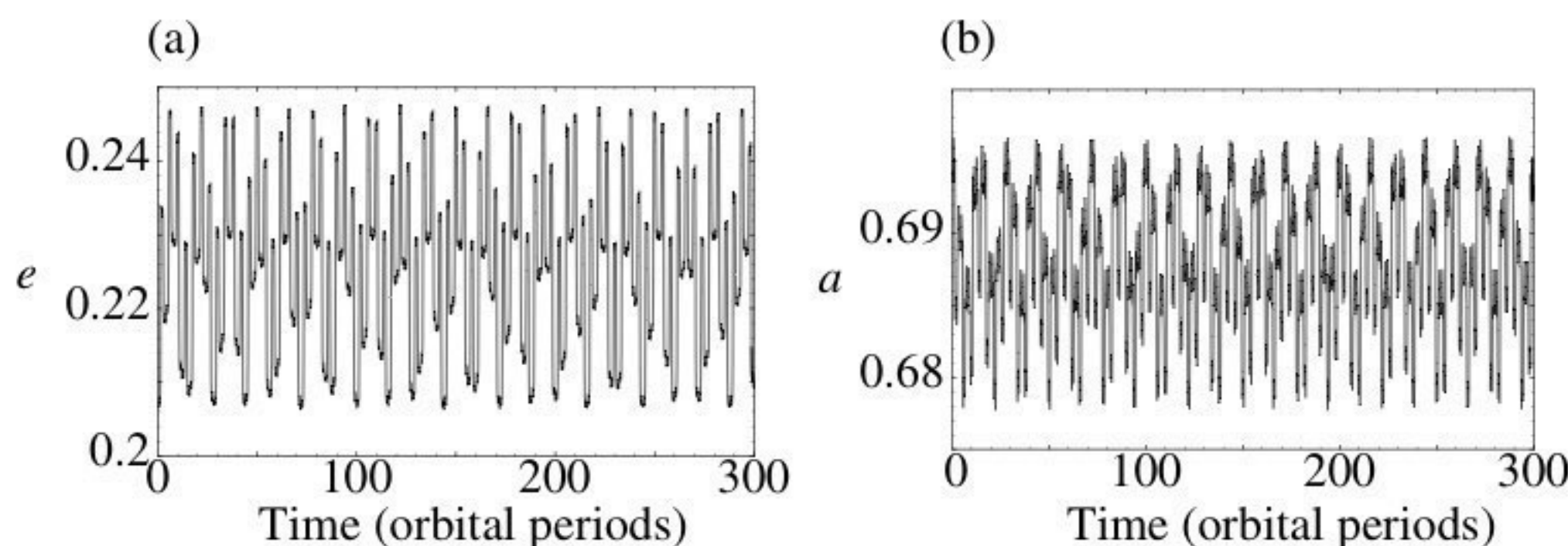


Fig. 9.4. The time variability of (a) eccentricity  $e$  and (b) semi-major axis  $a$  for initial values  $a_0 = 0.6944$  and  $e_0 = 0.2065$ . The plots show a behaviour characteristic of regular orbits. (Adapted from Murray 1998.)

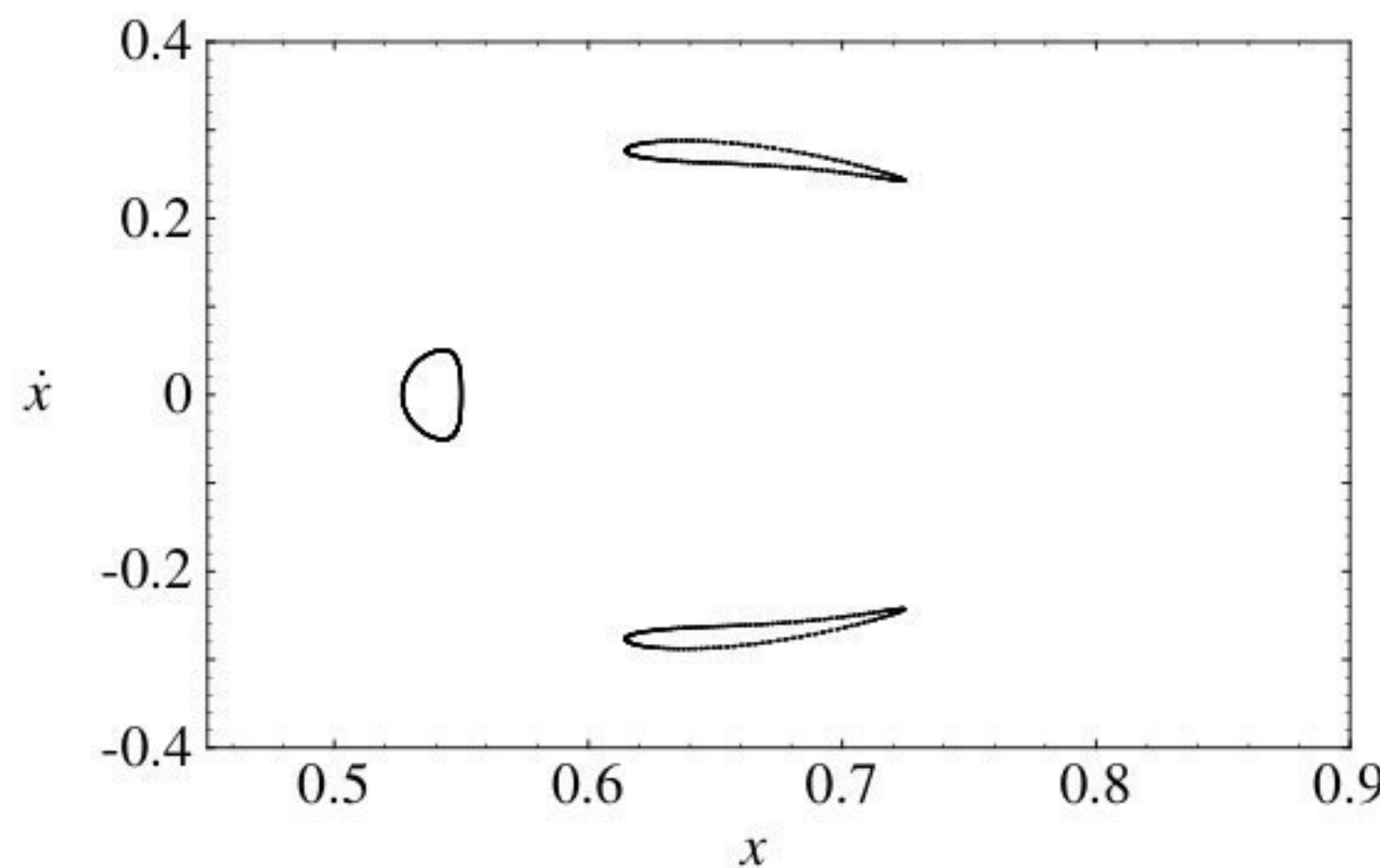


Fig. 9.5. A surface of section for the regular trajectory shown in Fig. 9.4. The points are plotted whenever  $y = 0$  with  $\dot{y} > 0$ . (Adapted from Murray 1998.)

range 0.206–0.248 over the course of the integration. At this particular location we would expect to see resonant perturbations since  $(a/a_J)^{3/2} = 0.564 \approx 4/7$  and the orbit of the test particle is close to a 7:4 resonance with Jupiter. The equivalent plot for the variation of the semi-major axis is shown in Fig. 9.4b. Note that the changes in  $a$  are correlated with those in  $e$ , as we would expect from some of the simple relations discussed in Sect. 8.5. The value of  $a$  appears to be librating close to the location of the nominal resonance at  $a = (4/7)^{2/3} \approx 0.689$ . Figure 9.4 only shows the variations in  $e$  and  $a$ . A complete description of the trajectory should also involve plots of  $\varpi$  and another angle, such as the mean longitude  $\lambda$ .

Figure 9.5 shows the same trajectory displayed as a surface of section, obtained by plotting the values of  $x$  and  $\dot{x}$  whenever  $y = 0$  with  $\dot{y} > 0$ . The pattern that emerges shows three, distinct “islands”. The appearance of such islands is one characteristic of resonant motion when displayed as a surface of section. In these cases a mean motion resonance of the form  $p + q : p$ , where  $p$  and  $q$  are integers, produces  $q$  islands. In this case  $p = 4$ ,  $q = 3$ , and three islands are visible. An important point to note is the manner in which these islands appear on the plot as the trajectory is followed. Rather than tracing out one island at a time, successive points occur at each of the three island locations in turn, until they appear to form three smooth curves.

If we choose a value of  $x_0$  that places the starting point at the centre of the island that straddles the  $\dot{x} = 0$  line, then the trajectory would appear as a succession of three points, one at the centre of each island in turn. This is because the centre of each island corresponds to a starting condition that places the test particle at the middle of the resonance. This is the type of resonant orbit illustrated in Fig. 8.15a for the 2:1 resonance. Such points are said to be periodic points of the Poincaré map because the system returns to the same point every third time

the trajectory crosses the section. By moving the starting location further away from the centre the islands would get larger, corresponding to larger variations in  $e$  and  $a$ . Eventually some starting values would lead to trajectories that were not in resonant motion and there would no longer be distinct islands in the section plot.

### 9.3.3 Chaotic Orbits

Figure 9.6 shows the plots of  $e$  and  $a$  as a function of time for the test particle orbit with starting values  $x_0 = 0.56$ ,  $y_0 = 0$ , and  $\dot{x}_0 = 0$ , and  $\dot{y}$  determined from Eq. (9.5) with  $C_J = 3.07$ , the same value used above to illustrate the regular trajectory. The corresponding orbital elements are  $a_0 = 0.6984$  and  $e_0 = 0.1967$ . Note that although these values are only slightly different from those used above, the nature of the variations in  $e$  and  $a$  are very different. The eccentricity undergoes irregular variations from 0.188 to 0.328 and the value of  $a$  does not remain close to the resonant value. This is a chaotic trajectory where there is no obvious pattern to the variations in the orbital elements; this alone does not necessarily mean that the orbit is chaotic. For example, a secular solution to the  $N$ -body problem can display complicated behaviour similar to that associated with chaotic motion and yet we know that it is derived from an analytical solution composed of a finite number of frequencies.

The identification of this particular orbit as chaotic becomes apparent from a study of its Poincaré surface of section (see Fig. 9.7). Note that the orbit covers a larger region of phase space than in the regular example (cf. Fig. 9.5). Furthermore, instead of the points lying on a smooth curve, they are beginning to fill an area of the phase space. Note also that there is a tendency for some points to “stick” to the edge of the 7:4 and other resonances; indeed the points

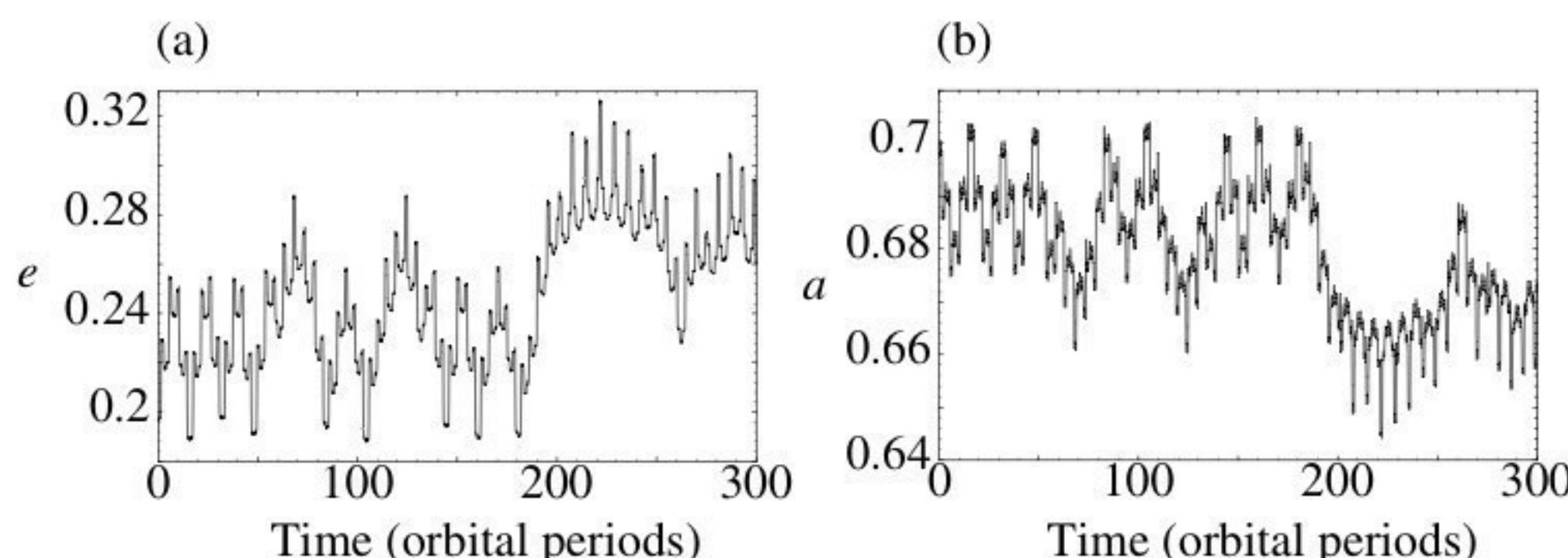


Fig. 9.6. The time variability of (a) eccentricity  $e$  and (b) semi-major axis  $a$  for initial values  $a_0 = 0.6984$  and  $e_0 = 0.1967$ . The plots show a behaviour characteristic of chaotic orbits. (Adapted from Murray 1998.)

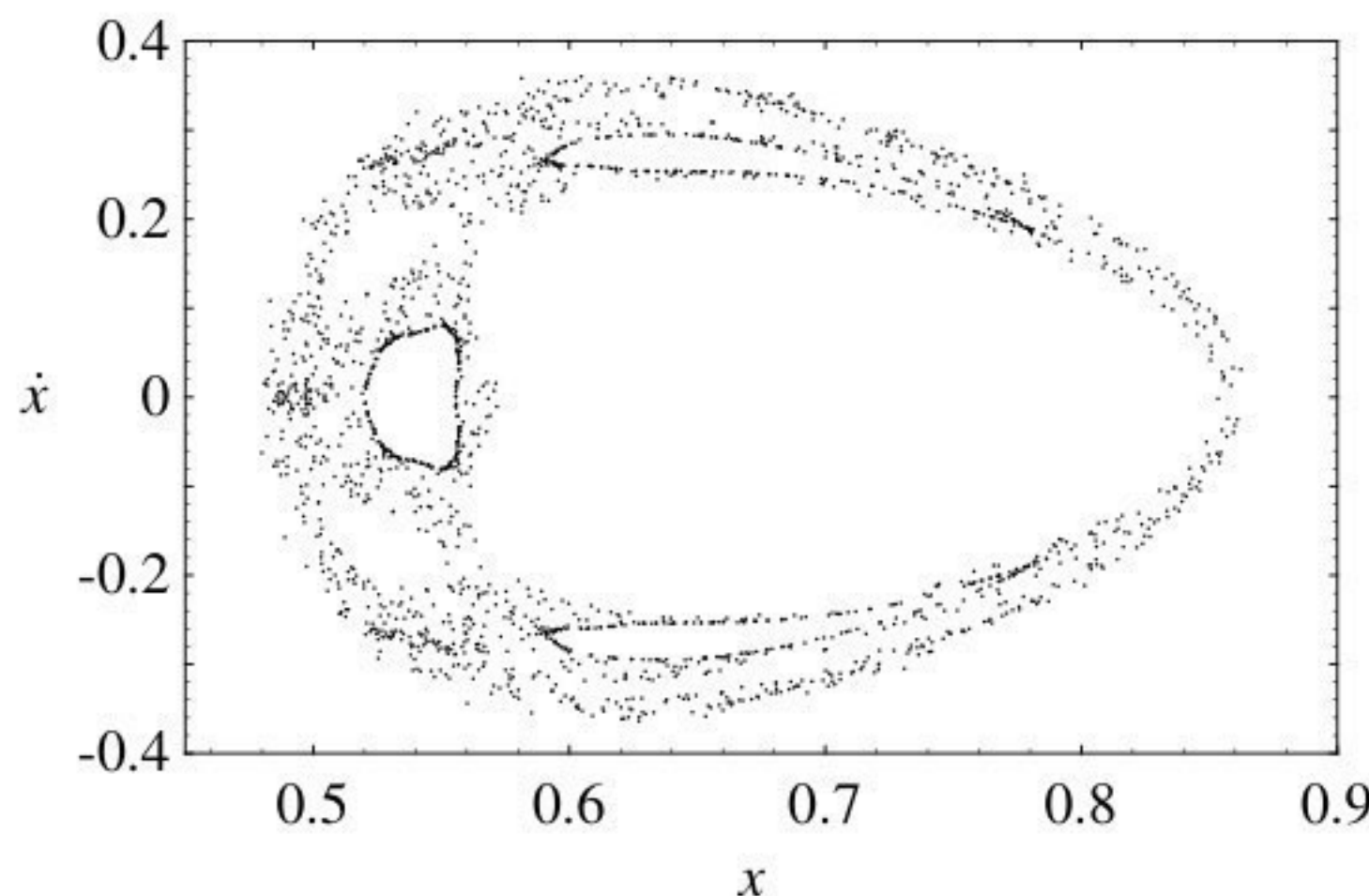


Fig. 9.7. A surface of section for the chaotic trajectory shown in Fig. 9.6. The points are plotted whenever  $y = 0$  with  $\dot{y} > 0$ , and the scale is the same as that in Fig. 9.5. (Adapted from Murray 1998.)

in the chaotic trajectory help to define several empty regions, each of which can be associated with a resonance. The stickiness phenomenon implies that if we examine the trajectory at particular times it may give the impression of regular motion. In fact, this is another characteristic of chaotic behaviour – it can give the impression of regular motion for long periods of time; this can make chaotic motion difficult to detect in some circumstances.

Although the chaotic orbit shown in Fig. 9.7 covers a large area of the  $x$ - $\dot{x}$  space, there is some evidence that there are still bounds to the motion. Thus, this orbit may illustrate the phenomenon of *bounded chaos* and this will be discussed in Sect. 9.4.

### 9.3.4 The Lyapounov Characteristic Exponent

Chaotic orbits have the characteristic that they are sensitively dependent on initial conditions. This is illustrated in Fig. 9.8 where we show part of the plot of  $e$  as a function of time for two similar chaotic trajectories. The first corresponds to the trajectory shown in Figs. 9.6 and 9.7 where we used  $x_0 = 0.56$ ; the second has  $x_0 = 0.56001$  and we have adjusted the initial value of  $\dot{y}$  to maintain the same value of  $C_J$ . It is clear that after 60 orbital periods the orbits have drifted apart. If we performed the same displacement experiment and followed the evolution of a regular orbit there would be some variation in the magnitude of the relative separation but we would not detect such a large drift.

We can make use of the type of divergence seen in Fig. 9.8 to measure the *maximum Lyapounov characteristic exponent* (LCE) of a dynamical system, giving us a quantitative measure of the rate of divergence of nearby trajectories (see, for example, Lichtenberg & Lieberman 1983). In a dynamical system such

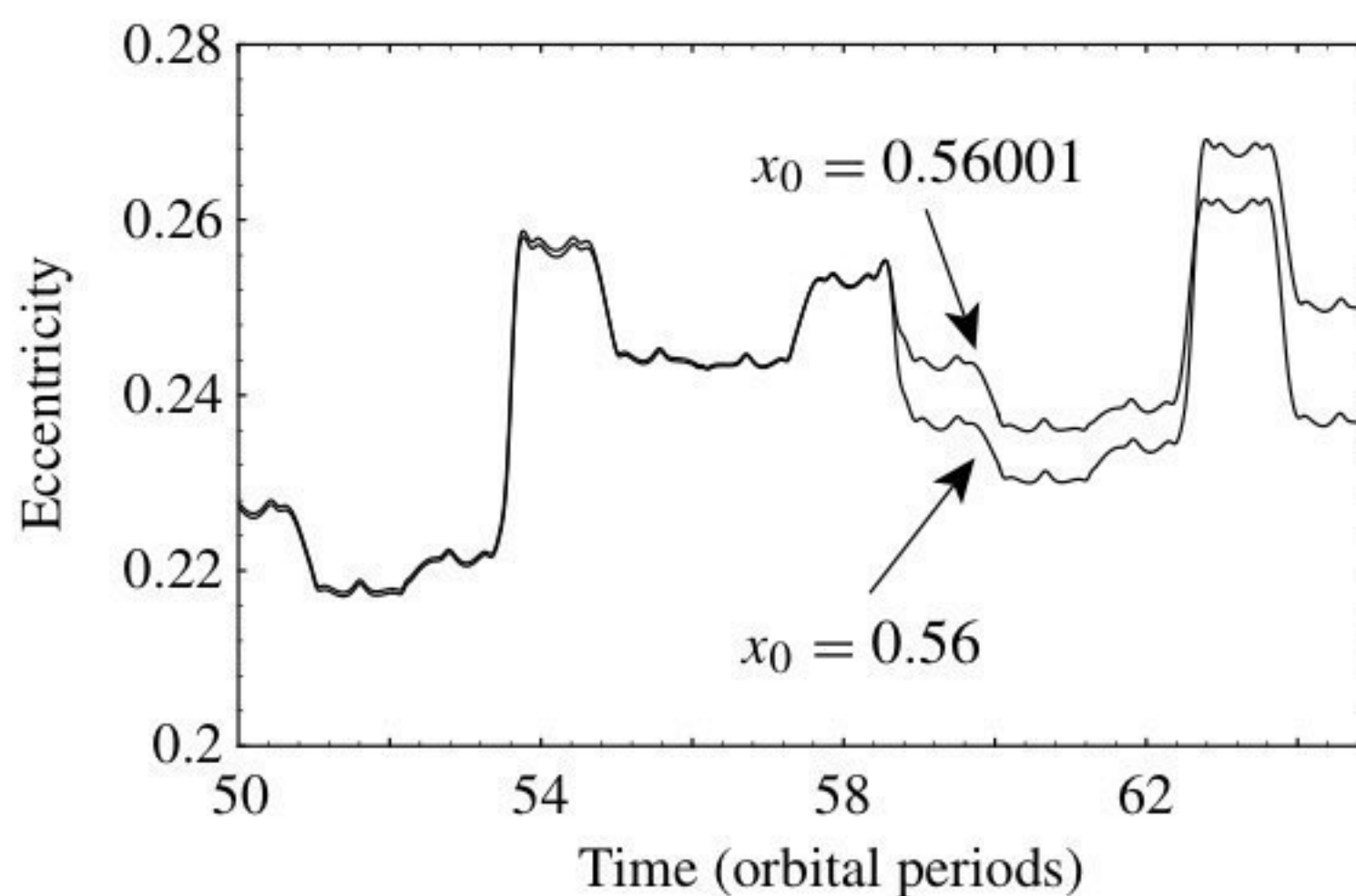


Fig. 9.8. Parts of two plots of the time evolution of the eccentricity for two nearby orbits in a chaotic region of the phase space. The initial values of  $x$  differ by 0.00001 and a clear separation can be seen after  $\sim 60$  orbital periods. (Adapted from Murray 1998.)

as the three-body problem there are a number of quantities called the Lyapounov characteristic exponents. For an arbitrary starting condition it can be shown that a measurement of the local divergence of nearby trajectories leads to an estimate of the largest of these exponents.

Consider two orbits separated in phase space by a distance  $d_0$  at time  $t_0$  (see Fig. 9.9a). Let  $d$  be their separation at time  $t$ . The orbit is chaotic if  $d$  is approximately related to  $d_0$  by

$$d = d_0 \exp \gamma(t - t_0), \quad (9.6)$$

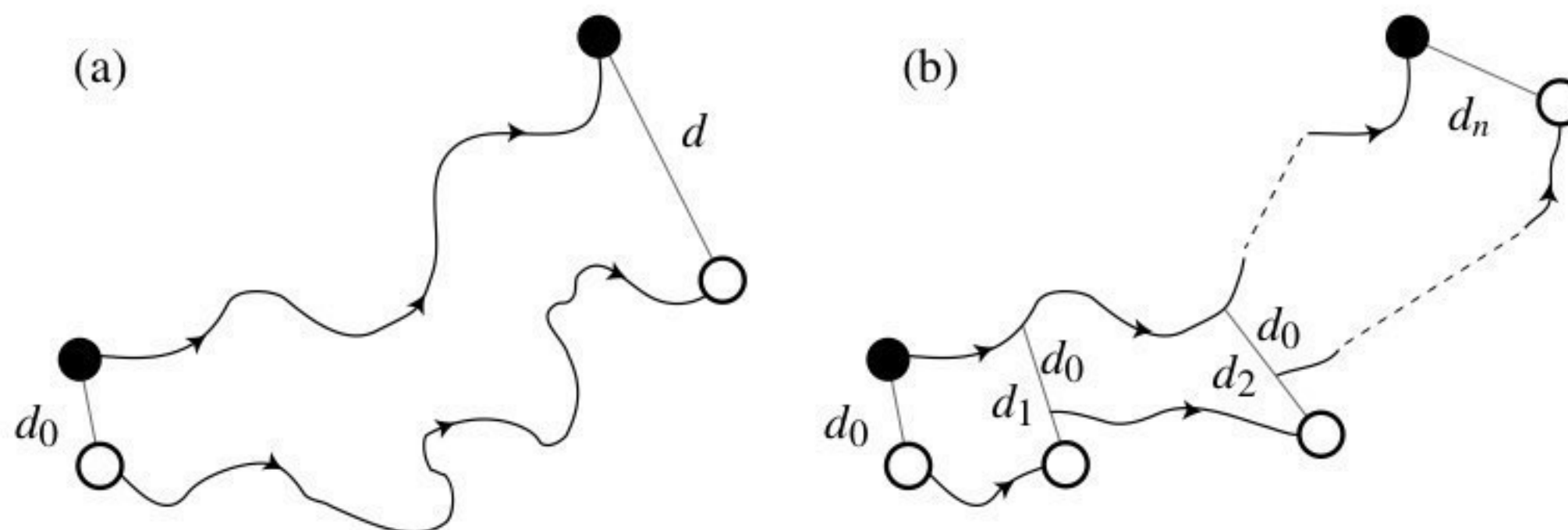


Fig. 9.9. Calculation of the maximum Lyapounov characteristic exponent by measuring the divergence of nearby trajectories. (a) The straightforward method of calculating the initial and final separations in phase space. (b) The renormalisation method whereby the displaced particle's trajectory is moved back along the separation vector to the original displacement distance.

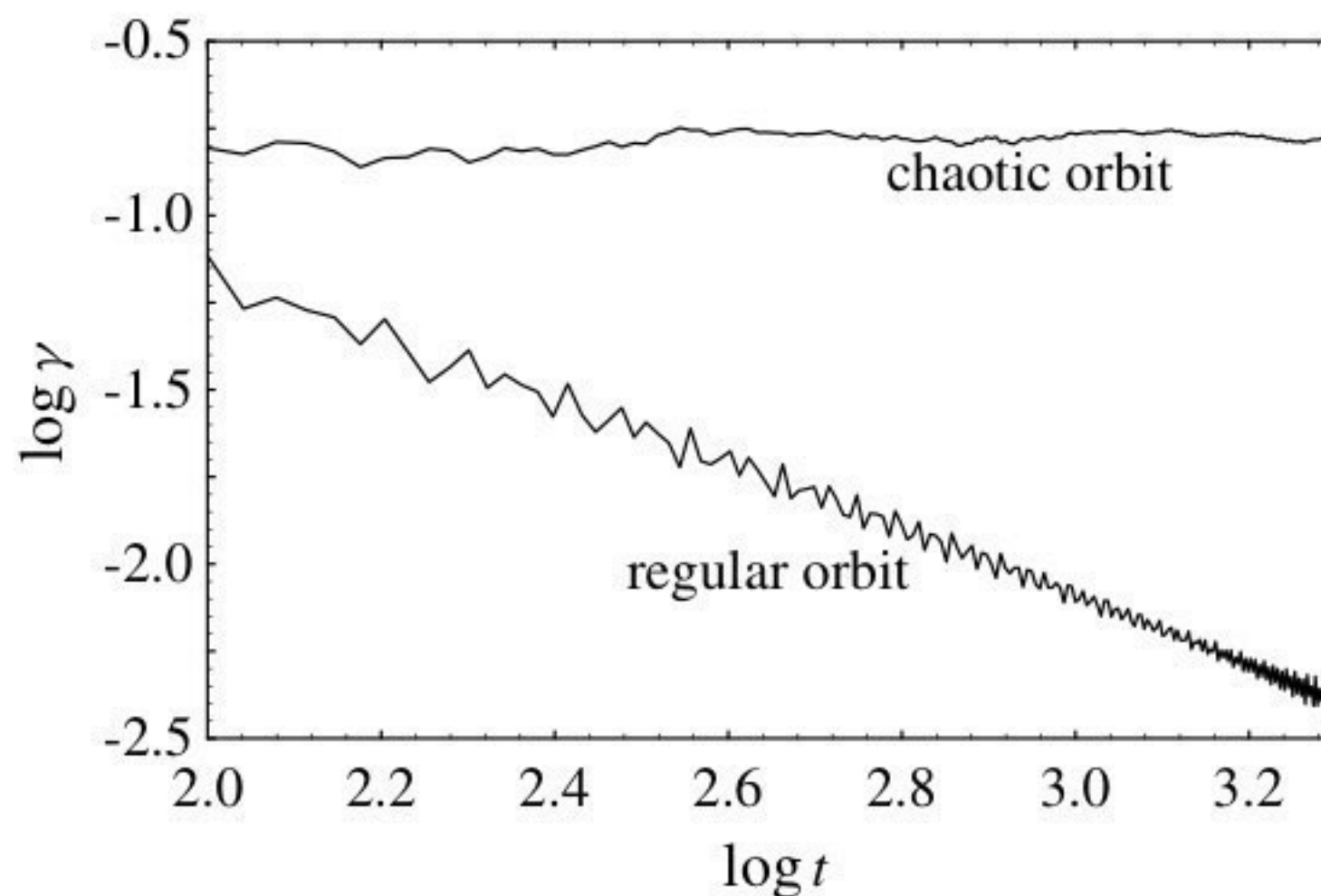


Fig. 9.10. Plots of  $\log \gamma$  as a function of  $\log t$  for the regular and chaotic trajectories discussed above. (Adapted from Murray 1998.)

where  $\gamma$  is the maximum Lyapounov characteristic exponent. Note that we must have  $\gamma > 0$  for otherwise the trajectories would approach one another as  $t$  increased. We can estimate the value of  $\gamma$  from the results of a numerical integration by means of the relation

$$\gamma = \lim_{t \rightarrow \infty} \frac{\ln(d/d_0)}{t - t_0}. \quad (9.7)$$

Monitoring the behaviour of  $\gamma$  as a function of time on a log–log scale usually reveals a striking difference between regular and chaotic trajectories. For regular orbits the initial and final displacements are close to one another ( $d \approx d_0$ ) and hence a log–log plot would have a slope of  $-1$ . However, if the orbit is chaotic, then  $\gamma$  tends to a positive value. In cases where the displaced trajectory drifts too far from the original one  $\gamma$  is no longer a measure of the local divergence of the orbits. Therefore it is advisable to rescale (or renormalise) the separation vector of the nearby trajectory at fixed time intervals,  $\Delta t$  (see Fig. 9.9b). If there are  $n$  such renormalisations then the revised estimate of  $\gamma$  is

$$\gamma = \lim_{n \rightarrow \infty} \sum_{i=1}^n \frac{\ln(d_i/d_0)}{n\Delta t}. \quad (9.8)$$

Figure 9.10 shows  $\log \gamma$  as a function of  $\log t$  for the sample regular and chaotic orbits described above. From this plot we can derive an estimate of  $\gamma = 10^{-0.77}$  (orbital periods) $^{-1}$  for the maximum Lyapounov characteristic exponent of the chaotic orbit. The corresponding *Lyapounov time*, the time for the displacement to increase by a factor  $e$ , is given by  $1/\gamma$ , which in this case is  $\sim 6$  orbital periods. Therefore, at least for this starting condition, the chaotic nature of the orbit quickly becomes apparent. This is consistent with the demonstration shown in Fig. 9.8.

For simpler dynamical systems it can be possible to obtain all the Lyapounov characteristic exponents by analytical means. However, this is usually the exception in solar system dynamics. Furthermore, numerical experiments that follow the evolution of two nearby orbits may not always be successful, since our approximation to the maximum LCE,  $\gamma$ , is only defined in the limit as  $t \rightarrow \infty$  or  $n \rightarrow \infty$ . For example, the phenomenon of some chaotic orbits sticking to the boundaries of resonances implies that there may be the appearance of a regular trajectory for long periods of time. Therefore, although the chaotic nature of a chaotic orbit may be readily apparent, it may never be possible to prove a regular orbit is truly regular.

## 9.4 Chaos in the Circular Restricted Problem

The planar, circular, restricted three-body problem is perhaps the simplest dynamical model that approximates the motion of real objects in the solar system and yet, as we have seen, it has orbital solutions that display a surprising degree of complexity. In the previous section we demonstrated the existence of regular and chaotic orbits for a small sample of orbits; yet the structure of the phase space in the circular restricted problem is far from being fully understood. In this section we consider some of the properties of the restricted problem for the specific mass ratio of  $\mu_2 = 10^{-3}$ , following the work of Winter & Murray (1994a,b). Note that for this value of  $\mu_2$  the results given here for the motion of test particles approximate the motion of asteroids perturbed by a coplanar Jupiter moving on a circular orbit.

There have been several numerical studies of the circular restricted problem (see, for example, Hénon 1969 and Jefferys 1971). In the comprehensive survey by Winter & Murray (1994a,b) several hundred surfaces of section were produced for a variety of Jacobi constants and orbits both internal and external to the orbit of the perturber were examined. From these plots it is possible to measure properties such as the location and size of regular and chaotic regions and the maximum amplitude of resonant librations.

Recall that in the restricted problem neither the orbital energy nor the angular momentum are conserved because the potential experienced by the particle is explicitly time dependent. However, the dynamical system retains an integral of the motion, the Jacobi constant, given by Eq. (9.5). As we saw in Chapter 3, setting  $\dot{x} = \dot{y} = 0$  in the definition of  $C_J$  results in an equation that describes the zero-velocity curves associated with the value of  $C_J$ . These curves define the limits of prohibited regions in the physical space since particles with that value of  $C_J$  cannot move inside such regions. Figure 9.11 shows zero-velocity curves and the corresponding regions from which the particle is excluded for a selection of values of  $C_J$ .